Parametric light bullets supported by quasi-phase-matched quadratically nonlinear crystals

N.-C. Panoiu* and R. M. Osgood, Jr.
Department of Applied Physics and Applied Mathematics, Columbia University, New York, New York 10027, USA

B. A. Malomed
Department of Interdisciplinary Studies, Faculty of Engineering, Tel-Aviv University, Tel-Aviv 69978, Israel

F. Lederer
Institute of Solid State Theory and Theoretical Optics, Friedrich Schiller University Jena, Max-Wien-Platz 1, Jena, D-07743, Germany

D. Mazilu and D. Mihalache
Department of Theoretical Physics, Institute of Atomic Physics, Horia Hulubei National Institute of Physics and Nuclear Engineering, P.O. Box MG-6, Bucharest, Romania

(Received 11 September 2004; published 18 March 2005)

We present a comprehensive analysis of the dynamics of three-dimensional spatiotemporal nonspinning and spinning solitons in quasi-phased-matched (QPM) gratings. By employing an averaging approach based on perturbation theory, we show that the soliton's stability is strongly affected by the QPM-induced third-order nonlinearity (which is always of a mixed type, with opposite signs in front of the corresponding self-phase and cross-phase modulation terms). We study the dependence of the stability of the spatiotemporal soliton (STS) on its energy, spin, the wave-vector mismatch between the fundamental and second harmonics, and the relative strength of the intrinsic quadratic and QPM-induced cubic nonlinearities. In particular, all the spinning solitons are unstable against fragmentation, while zero-spin STS's have their stability regions on the system's parameter space.

DOI: 10.1103/PhysRevE.71.036615 PACS number(s): 42.65.Tg, 42.65.Ky, 42.79.−e, 42.65.Sf

I. INTRODUCTION

Solitons are localized excitations that are not distorted upon propagation in a nonlinear medium. They can be found in many fields, such as optics, fluids, plasmas, condensed matter, and field-theory physics. Ever since their discovery, both fundamental physical properties and potential technological applications of the solitons have been attracting a steadily growing interest. In optical media, solitons form either through a balance between dispersive and self-phase-modulation (SPM) effects, as is the case of temporal solitons, or, in the spatial domain, as a result of the balance of diffraction and nonlinear self-focusing (for a historical perspective on optical solitons see Ref. [1]).

A paradigmatic example is provided by the optical solitons in silica fibers [2,3], in which case the transverse localization of the pulse is imposed by the fiber itself, whereas the longitudinal and temporal localizations are achieved by the perfect balance between the anomalous group-velocity dispersion (GVD) and SPM due to the Kerr effect in silica. Extending these ideas to the propagation in bulk [i.e., three-dimensional (3D) media] nonlinear dispersive media, one arrives at the concept of an optical spatiotemporal soliton (STS) [4,5] (alias "light bullets" [6]). However, a fundamental problem is that formal 3D solitons in uniform Kerr ($\chi^{(3)}$) media are strongly unstable, being subject to catastrophic wave collapse [7]. These theoretical challenges, as well as the fact that STS's could be used for potential applications in ultrafast all-optical logic devices [8], provided that they are formed at moderately low optical powers, have been a strong incentive for both theoretical considerations and experimental efforts.

Several approaches to stabilize the STS have been proposed. For example, one can employ media with a different nonlinear optical response: namely, saturable nonlinearity [9–11], self-induced transparency [12], cubic-quintic nonlinearity [13–15], or off-resonance two-level systems [16]. Alternatively, graded-index Kerr media can be used [17].

A different approach to generate stable STS's is to employ more than one propagating field, so that a 3D soliton would be formed through mutual dynamic trapping of the waves with different frequencies. The first example is the prediction of stable light bullets in quadratically nonlinear media [18–22], which is possible because the quadratic ($\chi^{(2)}$) nonlinearity does not lead to wave collapse in any physical dimension [4,23,24]. Also, stable "bullets" can be predicted in a more general case of an optical medium with competing $\chi^{(2)}$ and *self-defocusing* $\chi^{(3)}$ nonlinearities, which is sometimes referred to as the $\chi^{(2)}:\chi^{(3)}_{-}$ model [25]. In fact, optical STS's have been thus far observed experimentally solely in such a medium [26]. These experiments employed highly elliptical beams, such that diffraction effects were negligible in one transverse dimension; consequently, the observed STS's were $(2+1)$D light bullets (effectively, with two spatial and one temporal dimensions).

*Also with the Department of Theoretical Physics, Institute of Atomic Physics, Horia Hulubei National Institute of Physics and Nuclear Engineering, P.O. Box MG-6, Bucharest, Romania.

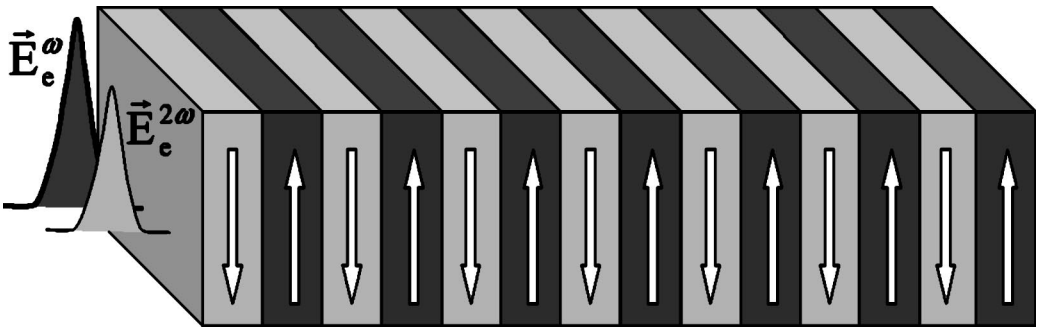

FIG. 1. Schematic of the SHG, in the QPM grating, under type-I conditions: two optical pulsed signals, with the electric fields $\mathbf{E}^{\omega}$ and $\mathbf{E}^{2\omega}$, polarized along the extraordinary axis, interact as they propagate in a grating with periodic variation of the quadratic susceptibility $\chi^{(2)}$. The arrows indicate the orientation of ferroelectric domains.

Vortex (spinning) solitons constitute a distinct class of STS's, in which the optical field carries angular momentum [15,25,27–31]. The vortex solitons have become the focus of rapidly growing interest, both because they offer ideal test objects to study fundamental properties of complex nonlinear excitations and due to promising possibilities for applications, such as trapping and channeling of matter waves, capturing and transport of microparticles, reconfigurable conduits for transmission of optical signals, and others. However, the stability is a more difficult issue for the spinning STS's, as compared to their zero-spin counterparts, chiefly because they are prone to strong instability against azimuthal perturbations. The first stable spinning STS's in (3+1)D dimensions have been predicted in the cubic-quintic [15] and $\chi^{(2)}:\chi^{(3)}_{-}$ [25] models. In both cases, stabilization is provided by the presence of *competing* (self-focusing and self-defocusing) nonlinearities.

Recently, it has been demonstrated both theoretically [32] and experimentally [33] that cascading of two-wave parametric frequency conversion in $\chi^{(2)}$ media may give rise an effective $\chi^{(3)}$ self-focusing or *self-defocusing* nonlinearity. Furthermore, by using the quasi-phase-matching (QPM) technique—i.e., compensation of the wave-vector mismatch through an additional wave vector induced by periodic reversal of the orientation of ferroelectric domains in the optical crystal— the highest $\chi^{(2)}$ coefficient may be used, making the two-wave parametric interaction most efficient. The QPM technique offers several other advantages: it eliminates spatial walk-off effects, nonbirefringent materials may be used, and the phase matching is achievable at room temperature.

For these reasons, QPM gratings may potentially be ideal media for both experimental and theoretical investigation of the multidimensional solitons. In particular, QPM-supported spatial solitons have been observed at intensities almost an order of magnitude lower than those required to generate them in bulk crystals [34]. Theoretical results for 1D [32,35–38], and 2D [39] QPM spatial solitons, in type-I systems, which employ two interacting waves (fundamental and second harmonics), polarized along the same direction, have also been reported. Recently, extensions to type-II systems, in which the parametric frequency conversion involves three waves, as the fundamental-frequency (FF) harmonic is a combination of two components with orthogonal polarizations, while the second-harmonic (SH) wave has a single polarization, have been reported for the 1D [40] and 2D [41] cases. These studies have shown, *inter alia*, that QPM induces an artificial cubic nonlinearity that may be self-defocusing, competing with the $\chi^{(2)}$ one, which is the necessary ingredient for generating stable spinning STS's. Furthermore, the induced $\chi^{(3)}$ nonlinearity can be further enhanced [37,42] by modulating the QPM grating; a switching scheme based on this effect has been proposed in Ref. [43].

In this paper, we present a theoretical investigation of the formation of spinning STS's, and their stability, in a bulk QPM grating. The paper is organized as follows. In the next section, we introduce the mathematical model that describes the interaction of copropagating waves in the type-I system. Then, in Sec. III we introduce the spinning STS's that can propagate in such a grating. A general discussion of the stability of the STS's is presented in Sec. IV, and a rigorous linear perturbation analysis of the stability is the subject of Sec. V. In the last section we summarize our results.

II. MATHEMATICAL MODEL

We consider the propagation of an optical pulse at frequency ω and its SH, at frequency 2ω, in a lossless bulk QPM grating, under type-I second-harmonic generation (SHG) conditions. The QPM grating is a periodic structure, in which both the linear part of the susceptibility—i.e., the refractive index—and the quadratic susceptibility $\chi^{(2)}$ are periodic functions of the longitudinal distance, as is illustrated in Fig. 1.

In this geometry, both the FF wave and the SH are polarized along the same direction, which is also a principal crystal axis; therefore, no walk-off effects are present. To describe a more general case, we allow for the average (normalized) quadratic susceptibility coefficient γ_0 to be nonzero, a situation that describes QPM gratings fabricated from semiconductor materials. Further, we assume that the relative index contrast of the grating is small.

The two interacting fields copropagate along the z direction and can be represented as

$$\mathbf{E}^{\omega_i}(\mathrm{r},t) = \tfrac{1}{2}\hat{\mathbf{e}}\mathcal{E}_i(x,y,z,t)\exp\left[i(\omega_i t - k_i z)\right] + \mathrm{c.c.}\,, \qquad (1)$$

where $\hat{\mathbf{e}}$ is a unit vector along the polarization direction, x and y are the transverse coordinates, z is the longitudinal

distance, t is time, and $\omega_n \equiv n\omega (n=1,2)$, $\mathcal{E}_i$ and $k_i = k(\omega_i)$ being the electric fields and wave vectors at the two harmonics, respectively. Then, within the slowly varying envelope approximation, the two copropagating fields obey the known equations [44],

$$2ik_1\left(\frac{\partial \mathcal{E}_1}{\partial z} + k_1'\frac{\partial \mathcal{E}_1}{\partial t}\right) + \nabla_\perp^2 \mathcal{E}_1 - k_1 k_1''\frac{\partial^2 \mathcal{E}_1}{\partial t^2} + \frac{2\omega_1^2 \bar{n}_1}{c^2}\Delta n_1(z)\mathcal{E}_1 + \frac{2\omega_1^2}{c^2}\chi^{(2)}(z)\mathcal{E}_1^* \mathcal{E}_2 e^{-i\Delta k z} = 0, \tag{2a}$$

$$2ik_2\left(\frac{\partial \mathcal{E}_2}{\partial z} + k_2'\frac{\partial \mathcal{E}_2}{\partial t}\right) + \nabla_\perp^2 \mathcal{E}_2 - k_2 k_2''\frac{\partial^2 \mathcal{E}_2}{\partial t^2} + \frac{2\omega_2^2 \bar{n}_2}{c^2}\Delta n_2(z)\mathcal{E}_2 + \frac{\omega_2^2}{c^2}\chi^{(2)}(z)\mathcal{E}_1^2 e^{i\Delta k z} = 0, \tag{2b}$$

where $\nabla_\perp^2$ is the transverse Laplacian, $\Delta k = 2k_1 - k_2$ is the wave-vector mismatch, $k_n' = (\partial k/\partial\omega)|_{\omega=\omega_n} = 1/v_{gn}$ is the inverse of the group velocity, $k_n'' = (\partial^2 k/\partial\omega^2)|_{\omega=\omega_n}$ is the GVD coefficient, and $\chi^{(2)}(z)$ is the z-dependent quadratic coefficient; $\bar{n}_1$, $\bar{n}_2$, and $\Delta n_1(z)$, $\Delta n_2(z)$ are, respectively, the average and the variable part (modulation) of the two refractive indices at the FF and SH. In order to normalize these equations, we define $\zeta = z/z_0$, $\xi = x/w_0, \eta = y/w_0$, $\tau = t/t_0$, $\Phi = A_1\mathcal{E}_1$, and $\Psi = A_2\mathcal{E}_2$. Here, $z_0 = k_1 w_0^2$ is the diffraction length at the FF, w_0 is the characteristic transverse spatial width of the pulse, $t_0 = \sqrt{z_0|k_1''|}$ is the characteristic pulse duration, and $A_i = \sqrt{\epsilon_0 c \bar{n}_i/2S_0}$ are normalization constants for the field amplitudes, with c being the speed of light, ϵ_0 the vacuum permittivity, and $S_0 = 1\mathrm{GW/cm}^2$ a normalization intensity. Upon the normalization, Eqs. (2) become

$$i\left(\frac{\partial \Phi}{\partial \zeta} + \vartheta_1\frac{\partial \Phi}{\partial \tau}\right) + \frac{1}{2}\left[\nabla_\perp^2 \Phi - \mathrm{sgn}(k_1'')\frac{\partial^2 \Phi}{\partial \tau^2}\right] + \alpha_\Phi(\zeta)\Phi + \Gamma(\zeta)\Phi^*\Psi e^{-i\beta\zeta} = 0, \tag{3a}$$

$$i\left(\frac{\partial \Psi}{\partial \zeta} + \vartheta_2\frac{\partial \Psi}{\partial \tau}\right) + \frac{1}{4}\left[\nabla_\perp^2 \Psi - \mathrm{sgn}(k_2'')\sigma\frac{\partial^2 \Psi}{\partial \tau^2}\right] + 2\alpha_\Psi(\zeta)\Psi + \Gamma(\zeta)\Phi^2 e^{i\beta\zeta} = 0, \tag{3b}$$

where $\vartheta_i = z_0/v_{gi}t_0$, $\beta = z_0\Delta k$ is the normalized wave-vector mismatch, $\alpha_{\Phi,\Psi}(\zeta) = \omega\Delta n_{1,2}(\zeta) z_0/c$ are the normalized modulations of the refractive indices [for a grating with uniform linear properties, $\alpha_{\Phi,\Psi}(\zeta) \equiv 0$ and $\gamma_0 = 0$], $\Gamma(\zeta) = (\omega\chi^{(2)} z_0/c)\sqrt{2S_0/\epsilon_0 c \bar{n}_1^2 \bar{n}_2}$ is the normalized parametric coupling strength, and $\sigma = 2|k_2''|/|k_1''|$. In deriving the system (3), we assumed that $2k_2 \approx k_1$, which is a good approximation for usual experimental conditions. Furthermore, we assume that the GVD at FF is anomalous in both media that form the QPM structure—i.e., $\mathrm{sgn}(k_1'') = -1$—in which case STS's exist, in the rigorous sense, only if the dispersion at SH is also anomalous or vanishes [19] (however, in some cases, STS's may "almost exist" even when the GVD is slightly normal at SH, which means that the soliton exists with a tiny, virtually invisible tail attached to it [45]). Therefore, we set $\mathrm{sgn}(k_2'') = -1$ and $\sigma \geqslant 0$. Thus, the two optical media that form the grating must have similar dispersion properties; therefore, the relative-GVD parameter σ is assumed constant along the grating.

The latter condition is rigorously satisfied by gratings obtained through the periodically poling of such ferroelectric materials as $LiNbO_3$ or $KTiOPO_4$ (KTP). Finally, it is assumed that the group velocities at the two harmonics are the same, $v_{g1} = v_{g2} \equiv v (\vartheta_1 = \vartheta_2)$, which means that there is no temporal walk-off between the two pulses. As a result, the first-order time derivatives in the system (3) can be eliminated by a simple transformation $\tau \to \tau - \zeta/v$.

The dynamics of the pulses is determined by the interplay of three characteristic lengths: the diffraction length z_0, the coherence length $L_c = \pi/|\Delta k|$, and the domain length of the grating, Λ. In the normalized units, $z_0 = 1$ and $L_c = \pi/|\beta|$. In typical experiments, the diffraction length is $z_0 \sim 1$ mm, whereas the domain length is $\Lambda \sim 10$ μm. Therefore, the approximation $\Lambda \ll 1$ holds, or, in other words, the grating's wave vector $|\Omega| = \pi/\Lambda$ is large, $|\Omega| \gg 1$. Furthermore, since the domain length is much larger than the wavelengths employed and the relative refractive index contrast between adjacent slabs in the grating is small, Bragg reflections may be neglected. Under these conditions, the dynamics of the beam interaction can be described by a set of averaged equations [32]. To derive them, we follow the method introduced in Ref. [32] (see also Refs. [39,41] for the case of 2D spatial solitons), Fourier-decomposing the grating parameters $\alpha_{\Phi,\Psi}(\zeta)$ and $\Gamma(\zeta)$,

$$\alpha_{\Phi,\Psi}(\zeta) = a_{\Phi,\Psi}\sum_n g_n e^{in\Omega\zeta}, \tag{4}$$

$$\Gamma(\zeta) = \gamma_0 + \gamma\sum_n g_n e^{in\Omega\zeta}, \tag{5}$$

and the fields $\Phi(\xi,\eta,\zeta,\tau)$ and $\Psi(\xi,\eta,\zeta,\tau)$,

$$\Phi(\xi,\eta,\zeta,\tau) = \sum_n \Phi_n(\xi,\eta,\zeta,\tau)e^{in\Omega\zeta}, \tag{6a}$$

$$\Psi(\xi,\eta,\zeta,\tau) = \sum_n \Psi_n(\xi,\eta,\zeta,\tau)e^{i(n\Omega+\bar{\beta})\zeta}, \tag{6b}$$

where γ_0 and γ are, respectively, the average value and modulation amplitude of the parametric-coupling strength, $\alpha_{\Phi,\Psi}$ are the amplitudes of the modulation of the refractive index, $\Phi_n(\xi,\eta,\zeta,\tau)$ and $\Psi_n(\xi,\eta,\zeta,\tau)$ are slowly varying functions of their arguments, as compared to $e^{i\Omega\zeta}$, and $\bar{\beta} = \beta - \Omega$ is the effective wave-vector mismatch parameter. We assume that the phase mismatch introduced by the grating can be accurately controlled; hence, $\bar{\beta}$ is very small (although both β and $|\Omega|$ are large). For the grating in Fig. 1, the Fourier coefficients $g_n = 2\mathrm{sgn}(\Omega)/i\pi n$ for odd n and $g_n = 0$ otherwise. Here, the $\mathrm{sgn}(\Omega)$ factor ensures that both positive and negative values of Ω correspond to the same grating. Consequently, since $\mathrm{sgn}(\beta) = \mathrm{sgn}(\Omega)$, we can treat both cases $\beta \lessgtr 0$ simultaneously. Furthermore, we assume that the higher-order harmonics in the expansions (6) are of order $\mathcal{O}(1/|\Omega|)$ or smaller, whereas the zero-order ones are of order $\mathcal{O}(1)$. Then, following the procedure introduced in Ref.

[32], we derive relationships between the higher-order Fourier coefficients and the zero-order ones (which are called *average fields* in this paper), Φ_0 and Ψ_0:

$$\Phi_{n\neq 0} = \frac{1}{n\Omega}[\alpha_\Phi g_n \Phi_0 + (\gamma_0 \delta_{n,-1} + \gamma g_{n+1})\Phi_0^* \Psi_0], \quad (7a)$$

$$\Psi_{n\neq 0} = \frac{1}{n\Omega}[2a_\Psi g_n \Psi_0 + (\gamma_0 \delta_{n,1} + \gamma g_{n-1})\Phi_0^2]. \quad (7b)$$

Further, by inserting these expressions in the system (3) and neglecting higher-order terms in the corresponding system that describes the evolution of the zero-order fields, we obtain the following system of equations that governs the dynamics of the zero-order (average) fields in the expansion (6):

$$i\frac{\partial \Phi_0}{\partial \zeta} + \frac{1}{2}\left(\nabla_\perp^2 \Phi_0 + \frac{\partial^2 \Phi_0}{\partial \tau^2}\right) + \rho \Phi_0^* \Psi_0 + \Delta(|\Phi_0|^2 - |\Psi_0|^2)\Phi_0 = 0, \quad (8a)$$

$$i\frac{\partial \Psi_0}{\partial \zeta} + \frac{1}{4}\left(\nabla_\perp^2 \Psi_0 + \sigma\frac{\partial^2 \Psi_0}{\partial \tau^2}\right) - \bar{\beta}\Psi_0 + \rho^* \Psi_0^2 - 2\Delta|\Phi_0|^2 \Psi_0 = 0, \quad (8b)$$

where the effective quadratic and induced cubic nonlinearities are represented by the parameters

$$\rho = \frac{2i\,\mathrm{sgn}(\Omega)}{\pi}[2\gamma_0(\alpha_\Phi - \alpha_\Psi)/\Omega - \gamma], \quad (9)$$

$$\Delta = [\gamma_0^2 + \gamma^2(1 - 8/\pi^2)]/\Omega. \quad (10)$$

Finally, by introducing the rescaled fields $u = |\rho|\Phi_0$ and $v = \rho\Psi_0$, the system (8) becomes

$$i\frac{\partial u}{\partial \zeta} + \frac{1}{2}\left(\nabla_\perp^2 u + \frac{\partial^2 u}{\partial \tau^2}\right) + u^* v + \delta(|u|^2 - |v|^2)u = 0, \quad (11a)$$

$$i\frac{\partial v}{\partial \zeta} + \frac{1}{4}\left(\nabla_\perp^2 v + \sigma\frac{\partial^2 v}{\partial \tau^2}\right) - \bar{\beta}v + u^2 - 2\delta|u|^2 v = 0, \quad (11b)$$

where $\delta = \Delta/|\rho|^2$ is the relative strength of the induced cubic nonlinearity and the intrinsic quadratic one. For typical QPM gratings, the latter parameter takes values $|\delta| \lesssim 0.05$, but as we will show later, even such small values can have a dramatic influence on the formation of STS's.

We stress that, unlike the full propagation system (8), the system (11) has constant coefficients, which greatly simplifies the analysis of existence and stability of its spinning STS solutions. It is also worthy to note that the form of the effective $\chi^{(3)}$ nonlinearity in Eqs. (11) is drastically different from that in the model which assumes a material Kerr nonlinearity, rather the artificial one [25]. In particular, the cubic nonlinear terms in Eqs. (11) are neither definitely self-focusing nor definitely self-defocusing, but are rather of a mixed kind. Indeed, if, for instance, δ is positive, the SPM term in the first equation is self-focusing, but the cross-phase modulation (XPM) terms in both equations are self-defocusing and the second equation includes no SPM term.

III. SPINNING SOLITONS IN THE QPM MEDIUM

To investigate the formation of spinning STS's in the bulk QPM grating, we proceed as follows. First, we find the spinning-soliton solutions of the average system (11) and subsequently use them to construct the spinning solitons that propagate in the actual QPM grating. For the latter step, we used the following relationships between the average fields $\{u, v\}$ and the actual ones $\{\Phi, \Psi\}$, which are valid to first order in $\epsilon = 1/|\Omega|$:

$$\Phi(\zeta = 0) = \frac{u(\zeta = 0)}{|\rho|} - \frac{1}{|\Omega|}\left[\frac{i\pi a_\Phi}{2} + \left(\frac{2i\gamma}{\pi} + \gamma_0 \mathrm{sgn}(\Omega)\right) \times \frac{v^*(\zeta = 0)}{\rho}\right]\frac{u(\zeta = 0)}{|\rho|} + \mathcal{O}\left(\frac{1}{|\Omega|^2}\right), \quad (12a)$$

$$\Psi(\zeta = 0) = \frac{v(\zeta = 0)}{\rho} - \frac{1}{|\Omega|}\left[i\pi a_\Psi \frac{v(\zeta = 0)}{\rho} + \left(\frac{2i\gamma}{\pi} - \gamma_0 \mathrm{sgn}(\Omega)\right)\frac{u^2(\zeta = 0)}{|\rho|^2}\right] + \mathcal{O}\left(\frac{1}{|\Omega|^2}\right). \quad (12b)$$

To derive these transformations one should insert the fields given by Eqs. (7) in the expansion (6) and collect all the terms up to the order $\mathcal{O}(1/|\Omega|^2)$.

To determine stationary spinning STS solutions of the system (11) we look for solutions that can be written as

$$u(\xi, \eta, \zeta, \tau) = U(r, \tau)e^{i\kappa\zeta + is\theta}, \quad (13a)$$

$$v(\xi, \eta, \zeta, \tau) = V(r, \tau)e^{2i\kappa\zeta + 2is\theta}, \quad (13b)$$

where U and V are assumed to be real functions, $r = \sqrt{\xi^2 + \eta^2}$ and θ are the polar coordinates in the transverse plane, κ is the soliton's propagation constant, and s is its vorticity ("spin"). Note that, although $U(r, \tau)$ and $V(r, \tau)$ describe stationary STS's, they satisfy a system of partial differential equations

$$\frac{1}{2}\left(\frac{\partial^2 U}{\partial r^2} + \frac{1}{r}\frac{\partial U}{\partial r} - \frac{s^2}{r^2}\frac{\partial^2 U}{\partial r^2} + \frac{\partial^2 U}{\partial \tau^2}\right) - \kappa U + UV + \delta(U^2 - V^2)U = 0, \quad (14a)$$

$$\frac{1}{4}\left(\frac{\partial^2 V}{\partial r^2} + \frac{1}{r}\frac{\partial V}{\partial r} - \frac{4s^2}{r^2}\frac{\partial^2 V}{\partial r^2} + \sigma\frac{\partial^2 V}{\partial \tau^2}\right) - (\bar{\beta} + 2\kappa)V + U^2 - 2\delta U^2 V = 0. \quad (14b)$$

Equations (14) have been solved numerically by using a standard band-matrix algorithm [46], for different values of the effective wave-vector mismatch $\bar{\beta}$, soliton's propagation constant κ, and relative-GVD parameter σ. Furthermore, to verify whether these spinning solitons preserve their shape upon propagation in the actual QPM grating, we used the

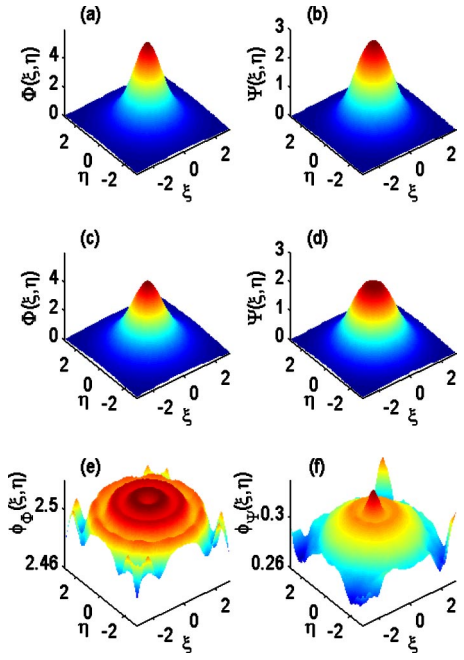

FIG. 2. (Color online) Field amplitude and phase profiles of the FF (left panels) and SH (right panels) waves, calculated in the cross section $\tau=0$, and corresponding to a zero-spin STS with the dispersion parameter $\sigma=1$, soliton wave vector $\kappa=0.5$, and zero wave-vector mismatch, $\bar{\beta}=0$. The field amplitude profiles are calculated at $\zeta=0$ [(a) and (b)] and $\zeta=20.164$ (30 grating periods) [(c) and (d)], whereas the phase profiles [(e) and (f)] are calculated at $\zeta=20.164$.

transformation (12) to restore the grating fields $\{\Phi,\Psi\}$ on the basis of the average ones, found by numerically solving Eqs. (14), and subsequently used these grating fields as initial conditions for the full propagation system (3). The latter system has been integrated by using a standard Crank-Nicolson method, with transparent boundary conditions [47] . For the parameters of the grating, we took $\alpha_\Phi=\alpha_\Psi=0$, $\gamma_0=0$, $\gamma=1$, and $\Omega=9.35$—i.e., a grating for which only the nonlinear susceptibility varies with the longitudinal distance ζ. The corresponding value of the induced $\chi^{(3)}$ coefficient is $|\delta|=0.05$.

One example that illustrates this procedure is presented in Fig. 2, which shows the FF and SH fields, in the cross section of $\tau=0$, both at the input facet of the QPM grating ($\zeta=0$) and after the propagation distance $\zeta=20.164$ (30 grating periods). In this case, the fields correspond to a zero-spin STS ($s=0$) with the relative-GVD parameter $\sigma=1$, propagation constant $\kappa=0.5$, and zero phase mismatch $\bar{\beta}=0$. Also shown in Fig. 2 are the phases of the two pulses at the output facet of the grating. This figure demonstrates that the soliton remains *stable* upon propagation, although its amplitude profile is slightly reshaped and the phases at both the FF and SH are weakly modulated.

To gain a deeper insight into the process of the STS formation in the actual QPM grating, we show in Fig. 3 the dependence of the total energy of the FF and SH components of the pulse versus the propagation distance. The soliton propagation is illustrated for three values of the dispersion parameter σ, $\sigma=0$, $\sigma=1$, and $\sigma=2$, and for both positive and

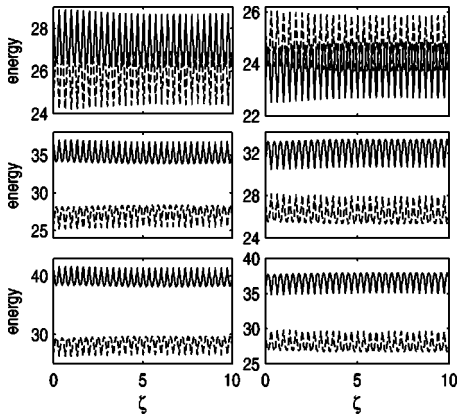

FIG. 3. The energy of the FF (solid lines) and SH (dashed lines) components vs the longitudinal distance ζ for $\delta=0.05$ (left panels) and $\delta=-0.05$ (right panels). The soliton parameters are $s=0$, $\kappa=0.1$, and $\bar{\beta}=0$ and the relative-GVD parameter $\sigma=0$ (upper panels), $\sigma=1$ (middle panels), and $\sigma=2$ (lower panels).

negative values of the relative $\chi^{(3)}$ strength parameter, $\delta=0.05$ and $\delta=-0.05$, respectively. In all three cases presented in Fig. 3, the solitons are characterized by parameter values $s=0$, $\kappa=0.1$, and $\bar{\beta}=0$. The energy of the FF and SH components, and the total energy are defined as follows:

$$E_\Phi=\int\int\int|\Phi(\zeta;\xi,\eta,\tau)|^2d\xi d\eta d\tau, \tag{15a}$$

$$E_\Psi=\int\int\int|\Psi(\zeta;\xi,\eta,\tau)|^2d\xi d\eta d\tau, \tag{15b}$$

$$E_{\rm tot}=E_\Phi+E_\Psi. \tag{15c}$$

Among other things, Fig. 3 shows that, after a short transient distance over which the input pulse gets reshaped, it attains a propagation regime in which, on average, the energies of its FF and SH components remain constant. Notice, however, that in this regime of quasistationary propagation, the soliton's amplitudes exhibit strong oscillations, a phenomenon that is a direct manifestation of the spatially periodic grating. Indeed, the period of oscillations in Fig. 3 exactly matches the periodicity of the grating.

The origin of the fast oscillations seen in Fig. 3 can be clarified if one resorts to the perturbative approach. Following the lines of the analysis developed in Refs. [32,39,41], one can derive relationships between the energies carried by the fields $\{\Phi,\Psi\}$ and the rescaled average ones, $\{u,v\}$, valid to the order $\mathcal{O}(1/|\Omega|^2)$:

$$E_\Phi=\frac{E_u}{|\rho|^2}+\frac{2iK}{\Omega|\rho|^2\rho}\left[\gamma_0\sin(\Omega\zeta)-\frac{4\,\mathrm{sgn}(\Omega)}{\pi}\sum_{n\geq1}\frac{\cos(2n\Omega\zeta)}{4n^2-1}\right]+\mathcal{O}\left(\frac{1}{|\Omega|^2}\right), \tag{16a}$$

$$E_\Psi = \frac{E_v}{|\rho|^2} - \frac{2iK}{\Omega|\rho|^2\rho}\left[\gamma_0 \sin(\Omega\zeta) - \frac{4\mathrm{sgn}(\Omega)}{\pi}\sum_{n\geqslant 1}\frac{\cos(2n\Omega\zeta)}{4n^2-1}\right] + \mathcal{O}\left(\frac{1}{|\Omega|^2}\right), \tag{16b}$$

where $K(\zeta)=\int\int\int u^2 v d\xi d\eta d\tau$ and the energies $E_{u,v}$ are given by expressions similar to Eqs. (15). Note that these relations hold only for real solutions $\{u,v\}$. When the average fields $\{u,v\}$ are stationary STS solutions of the system (11), K is a constant. Similar relations have been derived in Ref. [32], for the particular case of 1D gratings with $\gamma_0=0$. These equations show that fast modulations with spatial frequency 2Ω are superimposed on top of constant values of the energies, $E_{u,v}/|\rho|^2$. The origin of the modulations is the presence of higher-order terms in the Fourier expansion (6). Note that, if $\gamma_0\neq 0$, the spatial frequency of the modulation of the energies is equal to Ω. Also, notice that, up to a scaling transformation, the energies are conserved at the zeroth and first orders, $E_\Phi+E_\Psi=(E_u+E_v)/|\rho|^2$.

The induced third-order nonlinearity plays an important role in the dynamics of the STS's in the QPM. This conclusion is supported by the results obtained in the following numerical experiment. We found the solitons of the system (14) that correspond to $\bar{\beta}=0$, spin $s=0$ and $\delta=0,\pm 0.05$ for several values of the soliton propagation constant κ and relative-GVD parameter σ. Then, these solutions were used as initial conditions for the full dynamical equations (3), which were then integrated numerically until the average energy of the pulses would have reached a constant value. We then determined the ratio of the average peak intensities at the two harmonics and compared the results with those that correspond to the soliton solutions of the system (14). The results are presented in Fig. 4. As this figure illustrates, there is a large discrepancy between the predictions of the system (14), in which the third-order nonlinearity is taken into account ($\delta\neq 0$), and those with $\delta=0$. As one can see, for small values of the soliton's propagation constant κ, the former agree well with the numerical simulations of the full system (3). Note that the same behavior has been observed in the 1D model [32]. On the other hand, Fig. 4 also shows that, as κ increases, the predictions based on the average model become less accurate. The source of this discrepancy can be easily understood by noting that one of the conditions, under which the average model was derived, is that the average fields must vary slowly, as compared to $e^{i\Omega\zeta}$. This amounts to the requirement that κ must be much smaller than the grating's wave vector Ω. Importantly, Fig. 4 also shows that predictions based on the average model become more accurate if the relative-GVD parameter σ increases.

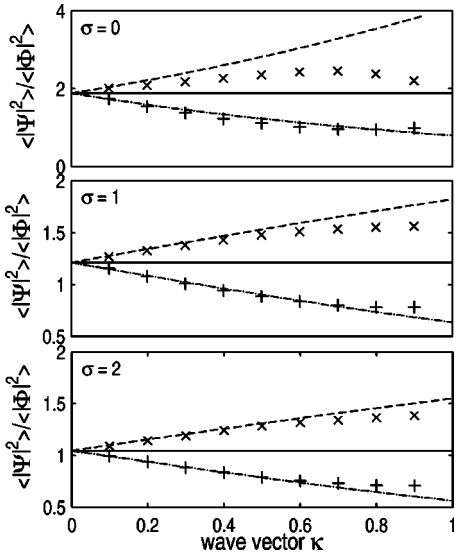

FIG. 4. Ratio between the peak intensities of the SH and FF components, $\langle|\Psi|^2\rangle/\langle|\Phi|^2\rangle$, of the soliton solutions of Eqs. (14), calculated for $\delta=-0.05$ (dashed lines), $\delta=0$ (solid lines), and $\delta=0.05$ (dot-dashed lines), vs soliton's propagation constant κ. The same ratio, which corresponds to the grating with $\delta=-0.05$ ($\times$) and $\delta=0.05$ (+), is shown as found by numerical integration of the full system 3 and averaging over ten diffraction lengths (see text for details). The parameters are $s=0$ (zero spin) and $\bar{\beta}=0$ (no wave-vector mismatch).

IV. GENERAL STABILITY PROPERTIES OF THE SPINNING STS

In this section, we present a general analysis of the stability properties of the STS's in the present model. In order to do this, we first determine the stability properties of the spinning STS solutions of the average system (11); then we investigate whether these stability characteristics are preserved when the spinning STS's propagate in the actual grating described by the full dynamical system (3). Note that the stability properties of the spinning STSs can also be investigated by employing a Floquet analysis of the plane-wave solutions of the full dynamical system (3) [36,38].

To this end, we define conserved quantities (integrals of motion) that are preserved by the dynamical equations (11): the total energy E, Hamiltonian H, and angular momentum L:

$$E = \int\int\int [|u(\xi,\eta,\zeta,\tau)|^2 + |v(\xi,\eta,\zeta,\tau)|^2] d\xi d\eta d\tau = E_u + E_v, \tag{17}$$

$$H = \frac{1}{2}\int\int\int \left[|\nabla_\perp u|^2 + \left|\frac{\partial u}{\partial\tau}\right|^2 + \frac{1}{4}|\nabla_\perp v|^2 + \frac{\sigma}{4}\left|\frac{\partial v}{\partial\tau}\right|^2 + (\bar{\beta}|v|^2 - u^{*2}v - u^2 v^*) - \delta(|u|^2 - 2|v|^2)|u|^2\right] d\xi d\eta d\tau, \tag{18}$$

$$L = \int\int\int \left(\frac{\partial\phi}{\partial\theta}|u(\xi,\eta,\tau)|^2 + \frac{\partial\psi}{\partial\theta}|v(\xi,\eta,\tau)|^2\right) d\xi d\eta d\tau, \tag{19}$$

where ϕ and ψ are the phases of the fields u and v, respectively. A simple consideration of the Eqs. (11) shows that, for stationary spinning STS solutions, the dynamical invariants

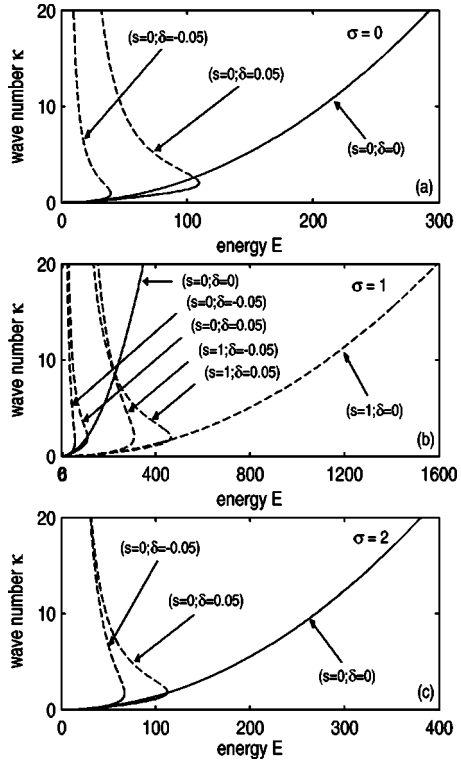

FIG. 5. The soliton's propagation constant κ vs the total energy E, calculated for the effective wave-vector mismatch $\bar{\beta}=0$. The solid and dashed curves correspond to stable and unstable soliton solutions, respectively.

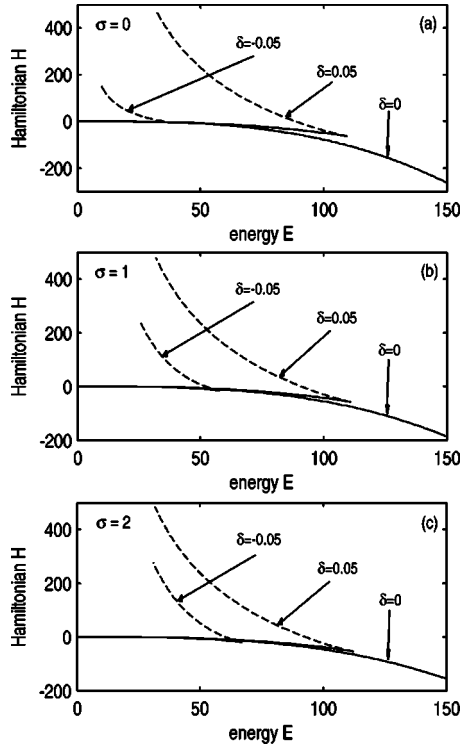

FIG. 6. The Hamiltonian H of the $s=0$ solitons, vs the total energy E, calculated for the effective wave-vector mismatch $\bar{\beta}=0$. The solid and dashed curves correspond to stable and unstable soliton solutions, respectively.

E, H, and L are related as follows: $L=sE$ and

$$H=\frac{1}{3}\left[\bar{\beta}E_u-\kappa E+\delta\int\int\int u^2(u^2-2v^2)d\xi d\eta d\tau\right]. \tag{20}$$

Equations (14) show that, for fixed system parameters $\bar{\beta}$, δ, and σ, which are defined by the experimental conditions, the spinning solitons with a given spin s form a one-parameter family of solutions. In addition, it is evident from Eqs. (14) that, to provide for the existence of spinning-soliton solutions, the soliton's propagation constant κ must obey the condition $\kappa\geqslant\kappa_{\text{cutoff}}=\max\{0,-\bar{\beta}/2\}$.

We have numerically computed both the nonspinning and spinning soliton solutions of the system (14), for the zero effective wave-vector mismatch parameter ($\bar{\beta}=0$) and for the relative-GVD parameters $\sigma=0$, $\sigma=1$, and $\sigma=2$; the results are summarized in Fig. 5, which shows the dependence of κ on the total energy E. In this figure, solid curves correspond to stable solutions, as discussed below, whereas the dashed ones represent unstable solutions. Figure 5 illustrates several important properties of the STS solutions. First, the nonspinning solitons ($s=0$) are stable in those parameter regions where the condition $dE/d\kappa>0$ holds, which is precisely the stability region predicted by the Vakhitov-Kolokolov (VK) criterion [48], which is a condition for the stability of a single-parameter family of solitons against perturbations with real eigenvalues (for this reason, in some cases the VK criterion indeed misses instability, if it is accounted for by complex eigenvalues [19,49]). In addition, for small absolute values of the $\chi^{(3)}$ parameter δ, $|\delta|\leqslant 0.05$, all the spinning solitons with $s=1$ are unstable, irrespective of the value of the relative-GVD parameter σ. Furthermore, Fig. 5 also shows that, if $\delta\neq 0$, for all the values of σ, the total energy of both stable solitons with $s=0$ and unstable ones with $s=1$ has an upper bound, whose value increases with δ. Generally, we observe that the parameter domain of stable solitons is larger in the case of $\delta>0$, which corresponds to the self-focusing SPM and self-defocusing XPM terms in the induced $\chi^{(3)}$ nonlinearity.

The conclusions derived from the dependence $\kappa=\kappa(E)$ are also supported by the diagram $H=H(E)$, which is shown in Fig. 6. The results displayed in this figure are in complete agreement with those derived from the $\kappa(E)$ dependence. In particular, if $\delta\neq 0$, the $H(E)$ diagram has two branches. This fact can also be derived from the analytical dependence of the Hamiltonian H on the energy E, given by Eq. (20), which suggests that, for $\bar{\beta}\leqslant 0$, there are two values of H that correspond to the same total energy E. Only the solitons on the lower branch are stable, as they correspond to a lower value of the Hamiltonian. Indeed, upon propagation, a soliton that corresponds to the upper branch (larger Hamiltonian for the same number of photons) ought to either completely decay into radiation or transform itself into a soliton belonging to the lower branch, shedding off some radiation. Direct simulations confirm this assumption.

V. LINEAR STABILITY ANALYSIS OF SPINNING STS's

Although the VK stability criterion offers a partial insight into the stability properties of the spinning STS solutions of Eq. (11), a full understanding of the stability of these states may only be provided by the linear stability analysis of the system (11), performed for small perturbations around stationary soliton solutions, in combination with direct simulations of the full dynamical equations. In this section, we present results of the linear stability analysis for the STS's as solutions to the average equations (11). These results will also be compared to direct simulations of the STS solutions in the full model of the QPM grating.

To begin with, we look for the growth rate λ_j of linear perturbation modes around the stationary solutions $U(r,\tau)$ and $V(r,\tau)$, within the framework of Eqs. (11) linearized around these solutions. The perturbed solutions are defined as follows:

$$u(\xi,\eta,\zeta,\tau) - U(r,\tau)e^{i(\kappa\zeta+s\theta)} = f(r,\tau)e^{\{\lambda_j\zeta+i[\kappa\zeta+(s+j)\theta]\}} + g^*(r,\tau)e^{\{\lambda_j^*\zeta+i[\kappa\zeta+(s-j)\theta]\}}, \tag{21a}$$

$$v(\xi,\eta,\zeta,\tau) - V(r,\tau)e^{2i(\kappa\zeta+s\theta)} = p(r,\tau)e^{\{\lambda_j\zeta+i[2\kappa\zeta+(2s+j)\theta]\}} + q^*(r,\tau)e^{\{\lambda_j^*\zeta+i[2\kappa\zeta+(2s-j)\theta]\}}, \tag{21b}$$

where $j \geqslant 0$ is an arbitrary integer azimuthal index of the perturbation, λ_j are eigenvalues (in the general case, they are complex), and the functions $f(r,\tau)$, $g(r,\tau)$, $p(r,\tau)$, and $q(r,\tau)$ represent the perturbation eigenmodes. These functions must obey the linear equations

$$i\lambda_j f + \frac{1}{2}\left[\frac{\partial^2 f}{\partial r^2} + \frac{1}{r}\frac{\partial f}{\partial r} - \frac{(s+j)^2}{r^2}\frac{\partial^2 f}{\partial r^2} + \frac{\partial^2 f}{\partial \tau^2}\right] - \kappa f + \delta(2U^2 - V^2)f + (U - \delta UV)p - \delta UVq + (V + \delta U^2)g = 0, \tag{22a}$$

$$-i\lambda_j g + \frac{1}{2}\left[\frac{\partial^2 g}{\partial r^2} + \frac{1}{r}\frac{\partial g}{\partial r} - \frac{(s-j)^2}{r^2}\frac{\partial^2 g}{\partial r^2} + \frac{\partial^2 g}{\partial \tau^2}\right] - \kappa g + \delta(2U^2 - V^2)g + (U - \delta UV)q - \delta UVp + (V + \delta U^2)f = 0, \tag{22b}$$

$$i\lambda_j p + \frac{1}{4}\left[\frac{\partial^2 p}{\partial r^2} + \frac{1}{r}\frac{\partial p}{\partial r} - \frac{(2s+j)^2}{r^2}\frac{\partial^2 p}{\partial r^2} + \sigma\frac{\partial^2 p}{\partial \tau^2}\right] - (2\kappa + \bar{\beta})p - 2\delta U^2 p + 2(U - \delta UV)f - 2\delta UVg = 0, \tag{22c}$$

$$-i\lambda_j q + \frac{1}{4}\left[\frac{\partial^2 q}{\partial r^2} + \frac{1}{r}\frac{\partial q}{\partial r} - \frac{(2s-j)^2}{r^2}\frac{\partial^2 q}{\partial r^2} + \sigma\frac{\partial^2 q}{\partial \tau^2}\right] - (2\kappa + \bar{\beta})q - 2\delta U^2 q + 2(U - \delta UV)g - 2\delta UVf = 0. \tag{22d}$$

Physical solutions of this system must decay exponentially at $r \to \infty$. Also, since the perturbation modes must be bounded at the origin, f and g must vanish as $r^{|s\pm j|}$ and p and q must vanish as $r^{|2s\pm j|}$, for $r \to 0$.

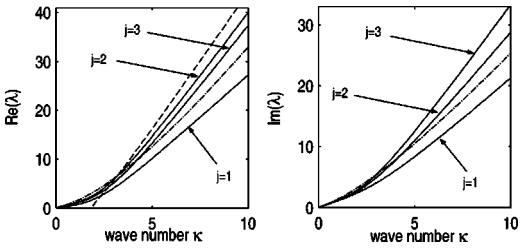

FIG. 7. The stability eigenvalues λ_j of the small perturbations around the spinning solitons with the effective phase mismatch $\bar{\beta}=0$ and relative-GVD parameter $\sigma=1$, found for several values of the azimuthal index j. The curves correspond to the following parameters: $s=0$, $j=0$, and $\delta=0.05$ (dashed lines), $s=1$ and $\delta=0.05$ (solid lines), and $s=1$, $j=2$, and $\delta=-0.05$ (dot-lines).

We have numerically found the eigenvalues λ_j and the corresponding eigenmodes of the system (22) by using a numerical method as in Ref. [50], which is based on direct integration of these equations by means of the Crank-Nicolson scheme. The results are summarized in Fig. 7. This figure shows that, for the range of values of the nonlinearity parameter δ investigated here—namely, $|\delta| \leqslant 0.05$—spinning solitons with $s=1$ are unstable for all κ. For $s=0$, the corresponding solitons are stable in the region of $0 \leqslant \kappa \leqslant \kappa_{\rm up}=1.93$. Note that, for $s=1$, all spinning solitons manifest an *oscillatory* instability ($\mathrm{Im}\lambda_j \neq 0$) [25,51–54], whereas for $s=0$ and $\kappa > \kappa_{\rm up}$, the unstable eigenvalues are real. These conclusions, concerning the soliton stability, fully agree with those suggested by Fig. 5(b), as described above.

We have checked the validity of these predictions by direct numerical simulations of both the average equations (11) and the full dynamical equations (3). To numerically integrate the systems (11) and (3), we used the Picard iteration method [47], and the resulting linear system of equations was solved by means of the Gauss-Seidel iterative scheme. The dynamical equations were discretized on a transverse grid with $141 \times 141 \times 141$ points, and a typical evolution step was $\Delta\zeta = 2.8 \times 10^{-3}$. Generally, six Picard iterations and six Gauss-Seidel iterations were sufficient to achieve a good convergence.

The main conclusion of our numerical simulations is that, for moderate values of the effective $\chi^{(3)}$ parameter $|\delta| \leqslant 0.05$, stable solitons of the average equations (11) are stable too upon propagation in the full QPM model (3) and, simultaneously, the unstable solitons of the average equations are also unstable in the full model. This means that the average system (11), combined with the linear stability analysis of its STS solutions, provides for a good framework to predict the behavior of the solitons upon propagation in the QPM grating.

In order to illustrate these results, in Fig. 8 we present the isosurfaces of the FF and SH fields for a soliton with $\bar{\beta}=0$, $\sigma=1$, $\delta=0.05$, $s=0$, and $\kappa=0.5$, taken at the input facet of the QPM grating, $\zeta=0$, and after they have passed 30 grating periods. The soliton parameters were chosen so that they correspond to a stable soliton solution of the system (11). This figure clearly shows stable propagation of the pulses, their final shape being undistorted as compared to the profile of the input pulses. Note that upon propagation the shape of

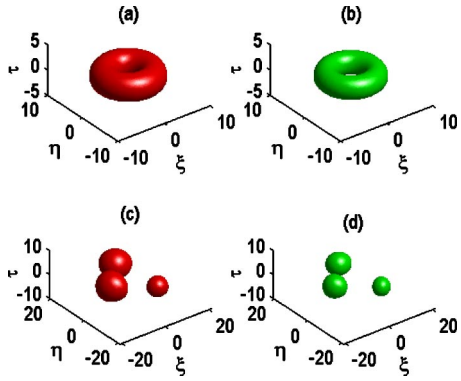

FIG. 9. (Color online) The same as in the previous figure, but in the case of an unstable spinning soliton, with $\bar{\beta}=0$, $\sigma=1$, $\delta=0.05$, $s=1$, and $\kappa=0.1$. The soliton suffers fragmentation, even though it was simulated using the simplified (averaged) equations (11). In the framework of the full system, the instability is still stronger (not shown here).

the pulses undergoes an oscillatory motion (see Fig. 3), which explains why the isosurfaces that correspond to the initial and final pulses shown in Fig. 8 have different sizes.

On the other hand, if unstable spinning solitons are considered, the behavior changes dramatically. This fact is illustrated in Fig. 9, which presents isosurface plots of the FF and SH fields of an unstable spinning soliton with parameters $\bar{\beta}=0$, $\sigma=1$, $\delta=0.05$, $s=1$, and $\kappa=0.1$, calculated at $\zeta=0$ and after a propagation distance of $\zeta=30$ grating periods. Note that, in this case, the soliton dynamics is simulated using the average system (11). Even within the framework of this simplified description, the propagation is clearly unstable, as the initial spinning soliton breaks in three fragments, which may be identified as zero-spin solitons. The splinters rotate around the longitudinal axis, so that total angular momentum is conserved. When the evolution of same spinning soliton is simulated using the equations of the full QPM model (the results are not shown here), it decays over a much shorter propagation distance, which suggests that the true instability is even stronger than predicted by the average equations.

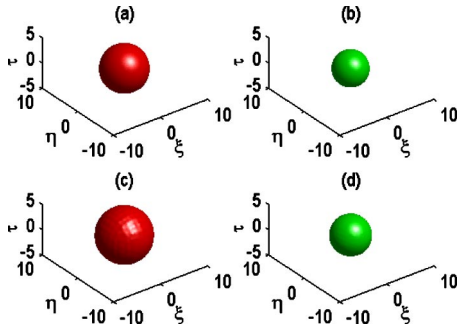

FIG. 8. (Color online) Isosurface plots of the FF (left panels) and SH (right panels) fields at $\zeta=0$ [(a) and (b)] and after the propagation distance equal to 30 grating periods [(c) and (d)]. The full model, based on Eqs. (3), was simulated here. The results illustrate stable propagation of a soliton with $\bar{\beta}=0$, $\sigma=1$, $\delta=0.05$, $s=0$, and $\kappa=0.5$.

VI. CONCLUSION

In this work, we have analyzed the $(3+1)$-dimensional spatiotemporal solitons, both nonspinning ($s=0$) and spinning ($s\neq 0$) ones, which propagate in bulk QPM gratings. We have considered both the case in which the grating has uniform linear optical properties—i.e., only the quadratic susceptibility changes along the propagation direction—and the more general case when, in addition to the optical nonlinearity, the linear optical coefficients, such as the refractive index and chromatic dispersion, weakly vary along the grating. Employing perturbation theory, we have demonstrated that the main characteristics of the STS dynamics in the QPM gratings are captured by an average model, which corresponds to a uniform optical medium that features both quadratic and effective (induced) cubic nonlinearities. The latter is neither self-focusing nor self-defocusing, but is rather of a mixed kind, featuring opposite signs in front of the SPM and XPM terms. Although the induced $\chi^{(3)}$ nonlinearities are small as compared to the intrinsic $\chi^{(2)}$ nonlinearity, they are large enough to strongly affect the dynamics of the STSs.

We have also investigated the stability of the solitons in detail. In particular, we have found that *all* the spinning solitons, with the spin $s\geqslant 1$, are *unstable* (at least, for values of the parameters that correspond to experimentally available conditions), whereas *stable* zero-spin solitons exist in a certain domain of the parameter space. In addition, our analysis has revealed that, if the SPM part of the induced $\chi^{(3)}$ nonlinearity is self-focusing, the size of this stability domain increases. We have verified the predictions for the solitons' stability, based on the linear perturbation analysis, by direct simulations of the soliton propagation in the full model of the QPM grating, as well as by numerical integration of the average dynamical equations. Good agreement between the different approaches was observed.

As a final comment, we stress that the results presented here are no longer valid if the two media forming the QPM grating have widely different optical properties. In particular, if the relative difference between the chromatic dispersion of the two media is large, the averaging procedure presented here no longer holds. In that case, one has to follow a different approach, using variational methods and/or direct simulations. Similar methods have been successfully used to describe the formation of localized optical pulses in Kerr layered media [55,56] or the existence of STSs in "tandem" structures, where the nonlinearity and GVD dispersion are concentrated in alternating slabs [57].

ACKNOWLEDGMENTS

The authors want to thank L. Torner for many useful discussions on QPM solitons. This work has been supported by the NIST Advanced Technology Program Cooperative Agreement No. 70NANB8H4018, and also in part by the AFOSR STTR, Grant No. FA9550-04-C-0022. D.M. and D.M. acknowledge financial support from Deutsche Forschungsgemeinschaft (DFG), Bonn. The work of B.A.M. is partly supported by the Israel Science Foundation though Grant No. 8006/03.

[1] G. A. Stegeman, D. N. Christodoulides, and M. Segev, IEEE J. Sel. Top. Quantum Electron. **6**, 1419 (2000).
[2] A. Hasegawa and F. Tappert, Appl. Phys. Lett. **23**, 142 (1973); **23**, 171 (1973).
[3] V. E. Zakharov and A. B. Shabat, Zh. Eksp. Teor. Fiz. **61**, 118 (1971) [Sov. Phys. JETP **34**, 62 (1972)]; **64**, 1627 (1973) [Sov. Phys. JETP **37**, 823 (1973)].
[4] A. A. Kanashov and A. M. Rubenchik, Physica D **4**, 122 (1981).
[5] J. T. Manassah, P. L. Baldeck, and R. R. Alfano, Opt. Lett. **13** 1090 (1988); J. T. Manassah, *ibid.* **16**, 563 (1991).
[6] Y. Silberberg, Opt. Lett. **15**, 1282 (1990).
[7] E. A. Kuznetsov, A. M. Rubenchik, and V. E. Zakharov, Phys. Rep. **142**, 103 (1986).
[8] R. McLeod, K. Wagner, and S. Blair, Phys. Rev. A **52**, 3254 (1995).
[9] D. E. Edmundson and R. H. Enns, Opt. Lett. **17**, 586 (1992); R. H. Enns and S. S. Rangnekar Phys. Rev. A **45**, 3354 (1992).
[10] N. Akhmediev and J. M. Soto-Crespo, Phys. Rev. A **47**, 1358 (1993).
[11] D. E. Edmundson, Phys. Rev. E **55**, 7636 (1997).
[12] M. Blaauboer, B. A. Malomed, and G. Kurizki, Phys. Rev. Lett. **84**, 1906 (2000).
[13] M. L. Quiroga-Teixeiro, A. Berntson, and H. Michinel, J. Opt. Soc. Am. B **16**, 1697 (1999).
[14] A. Desyatnikov, A. Maimistov, and B. Malomed, Phys. Rev. E **61**, 3107 (2000).
[15] D. Mihalache, D. Mazilu, L. C. Crasovan, I. Towers, A. V. Buryak, B. A. Malomed, L. Torner, J. P. Torres, and F. Lederer, Phys. Rev. Lett. **88**, 073902 (2002).
[16] I. V. Mel'nikov, D. Mihalache, and N. C. Panoiu, Opt. Commun. **181**, 345 (2000).
[17] S. Raghavan and G. P. Agrawal, Opt. Commun. **180**, 377 (2000).
[18] H. He, M. J. Werner, and P. D. Drummond, Phys. Rev. E **54**, 896 (1996).
[19] B. A. Malomed, P. Drummond, H. He, A. Berntson, D. Anderson, and M. Lisak, Phys. Rev. E **56**, 4725 (1997).
[20] D. V. Skryabin and W. J. Firth, Opt. Commun. **148**, 79 (1998).
[21] D. Mihalache, D. Mazilu, B. A. Malomed, and L. Torner, Opt. Commun. **152**, 365 (1998).
[22] D. Mihalache, D. Mazilu, J. Dorring, and L. Torner, Opt. Commun. **159**, 129 (1999).
[23] L. Berge, V. K. Mezentsev, J. J. Rasmussen, and J. Wyller, Phys. Rev. A **52**, R28 (1995).
[24] L. Berge, O. Bang, J. J. Rasmussen, and V. K. Mezentsev, Phys. Rev. E **55**, 3555 (1997).
[25] D. Mihalache, D. Mazilu, L. C. Crasovan, I. Towers, B. A. Malomed, A. V. Buryak, L. Torner, and F. Lederer, Phys. Rev. E **66**, 016613 (2002).
[26] X. Liu, L. J. Qian, and F. W. Wise, Phys. Rev. Lett. **82**, 4631 (1999); X. Liu, K. Beckwitt, and F. Wise, Phys. Rev. E **62**, 1328 (2000).
[27] G. A. Swartzlander and C. T. Law, Phys. Rev. Lett. **69**, 2503 (1992); A. W. Snyder, L. Poladian, and D. J. Mitchell, Opt. Lett. **17**, 789 (1992); D. Rozas, C. T. Law, and G. A. Swartzlander, J. Opt. Soc. Am. B **14**, 3054 (1997); B. Luther-Davies, J. Christou, V. Tikhonenko, and Yu. S. Kivshar, *ibid.* **14**, 3045 (1997).
[28] M. Quiroga-Teixeiro and H. Michinel, J. Opt. Soc. Am. B **14**, 2004 (1997).
[29] D. Mihalache, D. Mazilu, L. C. Crasovan, B. A. Malomed, and F. Lederer, Phys. Rev. E **61**, 7142 (2000).
[30] D. Mihalache, D. Mazilu, L. C. Crasovan, B. A. Malomed, and F. Lederer, Phys. Rev. E **62**, R1505 (2000).
[31] D. Mihalache, D. Mazilu, I. Towers, B. A. Malomed, and F. Lederer, Phys. Rev. E **67**, 056608 (2003).
[32] C. B. Clausen, O. Bang, and Y. S. Kivshar, Phys. Rev. Lett. **78**, 4749 (1997); J. F. Corney and O. Bang, Phys. Rev. E **64**, 047601 (2001).
[33] P. Di Trapani, A. Bramati, S. Minardi, W. Chinaglia, C. Conti, S. Trillo, J. Kilius, and G. Valiulis, Phys. Rev. Lett. **87**, 183902 (2001).
[34] B. Bourliaguet, V. Couderc, A. Barthelemy, G. W. Ross, P. G. R. Smith, D. C. Hanna, and C. De Angelis, Opt. Lett. **24**, 1410 (1999).
[35] C. B. Clausen, Y. S. Kivshar, O. Bang, and P. L. Christiansen, Phys. Rev. Lett. **83**, 4740 (1999).
[36] O. Bang and J. F. Corney, Opt. Photonics News **12**, 42 (2001); J. F. Corney and O. Bang, J. Opt. Soc. Am. B **19**, 812 (2002).
[37] S. K. Johansen, S. Carrasco, L. Torner, and O. Bang, Opt. Commun. **203**, 393 (2002).
[38] J. F. Corney and O. Bang, Phys. Rev. Lett. **87**, 133901 (2001); J. Opt. Soc. Am. B **21**, 617 (2004).
[39] N. C. Panoiu, D. Mihalache, D. Mazilu, F. Lederer, and R. M. Osgood, Phys. Rev. E **68**, 016608 (2003).
[40] N. C. Panoiu, D. Mihalache, H. Rao, and R. M. Osgood, Phys. Rev. E **68**, 065603(R) (2003).
[41] N. C. Panoiu, D. Mihalache, D. Mazilu, F. Lederer, and R. M. Osgood, J. Opt. B: Quantum Semiclassical Opt. **6**, S351 (2004).
[42] O. Bang, C. B. Clausen, P. L. Christiansen, and L. Torner, Opt. Lett. **24**, 1413 (1999).
[43] A. Kobyakov, F. Lederer, O. Bang, and Y. S. Kivshar, Opt. Lett. **23**, 506 (1998); O. Bang, T. W. Graversen, and J. F. Corney, *ibid.* **26**, 1007 (2001).
[44] C. R. Menyuk, R. Schiek, and L. Torner, J. Opt. Soc. Am. B **11**, 2434 (1994).
[45] I. N. Towers, B. A. Malomed, and F. W. Wise, Phys. Rev. Lett. **90**, 123902 (2003).
[46] G. Dahlquist and A. Bjork, *Numerical Methods* (Prentice Hall, Englewood Cliffs, NJ, 1974).
[47] J. M. Ortega and W. C. Rheinboldt, *Iterative Solution of Nonlinear Equations in Several Variables* (Academic Press, New York, 1970), p. 182.
[48] M. G. Vakhitov and A. A. Kolokolov, Radiophys. Quantum Electron. **16**, 783 (1973).
[49] O. Bang, Y. S. Kivshar, A. V. Buryak, A. De Rossi, and S. Trillo, Phys. Rev. E **58**, 5057 (1998).
[50] N. N. Akhmediev, V. I. Korneev, and Yu. V. Kuzmenko, Zh. Eksp. Teor. Fiz. **88**, 107 (1985) [Sov. Phys. JETP **61**, 62 (1985)]; J. M. Soto-Crespo, D. R. Heatley, E. M. Wright, and N. N. Akhmediev, Phys. Rev. A **44**, 636 (1991); W. J. Firth and D. V. Skryabin, Phys. Rev. Lett. **79**, 2450 (1997).
[51] N. N. Akhmediev, A. Ankiewicz, and H. T. Tran, J. Opt. Soc. Am. B **10**, 230 (1993).
[52] D. Mihalache, D. Mazilu, and L. Torner, Phys. Rev. Lett. **81**, 4353 (1998); D. Mihalache, D. Mazilu, and L. C. Crasovan, Phys. Rev. E **60**, 7504 (1999).
[53] I. V. Barashenkov, D. E. Pelinovsky, and E. V. Zemlyanaya,

Phys. Rev. Lett. **80**, 5117 (1998); A. De Rossi, C. Conti, and S. Trillo, *ibid.* **81**, 85 (1998); J. Schollmann, R. Scheibenzuber, A. S. Kovalev, A. P. Mayer, and A. A. Maradudin, Phys. Rev. E **59**, 4618 (1999).

[54] D. Mihalache, D. Mazilu, B. A. Malomed, and F. Lederer, Phys. Rev. E **69**, 066614 (2004).

[55] L. Berge, V. K. Mezentsev, J. J. Rasmussen, P. L. Christiansen, and Yu. B. Gaididei, Opt. Lett. **25**, 1037 (2000).

[56] I. Towers and B. A. Malomed, J. Opt. Soc. Am. B **19**, 537 (2002).

[57] L. Torner, S. Carrasco, J. P. Torres, L. C. Crasovan, and D. Mihalache, Opt. Commun. **199**, 277 (2001).